MAGNETIC FIELD ENHANCED THERMAL CONDUCTIVITY ANALYSIS OF MAGNETIC NANOFLUIDS

by

CHRISTOPHER ALLEN

Presented to the Faculty of the Graduate School of

The University of Texas at Arlington in Partial Fulfillment

of the Requirements

for the Degree of

MASTER OF SCIENCE IN MECHANICAL ENGINEERING

THE UNIVERSITY OF TEXAS AT ARLINGTON

December 2015

Acknowledgements

Many heartfelt thanks to Dr. Hyejin Moon for advising and instructing me through this research and writing process, and to my laboratory colleagues: Ali Farzbod, Shubhodeep Paul, Ajinkya Shetye, Mun Mun Nahar, and Dr. Shreyas Govindraj, for all your support and encouragement. Additional thanks to Dr. Ankur Jain and Dr. Ratan Kumar for serving on my defense committee.

November 24, 2015

Abstract

MAGNETIC FIELD ENHANCED THERMAL CONDUCTIVITY ANALYSIS OF MAGNETIC NANOFLUIDS

Christopher Allen, MS

The University of Texas at Arlington, 2015

Supervising Professor: Hyejin Moon

The magnetic properties of four water-based nanofluids consisting of Al2O3, CuO, Fe3O4, and SiO2 were exploited to analyze the effect of the application of an external magnetic field on the thermal conductivity of the nanofluid. When the magnetic field is applied, the magnetic dipole moments of the particles align and the particles come in contact with each other and form chains in the direction of the applied magnetic field. When parallel to the direction of heat flow, the magnetic field causes the effective thermal conductivity in the direction of the magnetic field to increase. A higher thermally conductive fluid can be applied to solve numerous heat transfer problems.

Table of Contents

List of Illustrations

List of Tables

Chapter 1

Introduction

1.1 – Nanofluids

Nanofluids are comprised of a concentration of nanoscale sized particles immersed in a base fluid. The particles can be composed of any type of material. Examples include pure metals, oxides, carbides, and carbon nanotubes. The base fluid can be anything from pure water, ionic liquids, oils, to diluted organic compounds such as ethylene glycol and oleic acid.[1] The addition of nanoparticles in these fluids cause this composite liquid to have tunable properties, which makes them extremely versatile substances. Nanoscale particles have an advantage over larger particles in such a way that, due to their small sizes, the effect of surface tension can overcome buoyant forces on each particle with the help of a surfactant, causing them to be suspended in the liquid rather than sinking to the bottom, which would be the case for microscale or larger particles. Thus, we can treat the flow of these nanofluids as a single-phase flow with consideration of the properties of both constituents and the concentration of nanoparticles in the fluid.[2] The properties and characteristics of these fluids have been widely researched and tested in a wide variety of applications. There have been experiments conducted to determine various thermal properties of nanofluids, such as specific heat and thermal conductivity, as well as rheological experiments conducted in order to determine the viscosity of different concentrations of nanofluids and their effect on fluid flow.

Given that nanofluids contain both solid and liquid constituents, there are certain attributes that nanofluids have that normal liquids do not, as they have both solid and liquid properties. We can exploit the solid properties such as their kinematic, inertial, magnetic attributes and particle size in order to control the properties of the bulk fluid. Since the particles are on the order of several nanometers in size, the atoms on the surface of the particle make up a larger portion of their mass than particles on the microscale or larger. Therefore, heat transfer through these particles will occur rather quickly, given that the thermal conductivity of the particles is much larger than their corresponding base fluid. Fluids generally do not conduct heat well, so the addition of particles will significantly enhance the effective thermal conductivity of the nanofluid as a whole.

1.2 – Thermal Properties

In conduction, heat flows through molecular vibrations in a material. The rate that heat flows through a material correlates with a temperature gradient; a relation that is known as Fourier's Law of Conduction. Heat always flows from a higher temperature to a lower temperature.

$$\vec{\mathbf{q}}'' = -k\,\vec{\nabla}T \tag{1.1}$$

Fourier's Law defines the heat flux in a material as linearly proportional to the temperature gradient inside the material. This proportionality constant k is known as the thermal conductivity. The thermal conductivity of a material is a measure of how fast heat flow by conduction occurs through it given a temperature gradient.

When the nanofluid is stationary, the particles are randomized within the base fluid, similar to a porous material with pores randomized throughout the material. Instead of defining the thermal conductivity for a fluid with beads of solid material contained within it, we swap the solid and fluid properties in the equation for the total effective thermal conductivity of a porous material, known as the Maxwell equation.[3]

$$k_0 = \left[\frac{k_s + 2k_f - 2\phi(k_f - k_s)}{k_s + 2k_f + \phi(k_f - k_s)}\right] k_f \tag{1.2}$$

Instead of using a porosity ϵ, we use the volume fraction of particles in the nanofluid, ϕ. When $\phi = 0$, we can see that the effective thermal conductivity will equal that of the fluid, k_f. Conversely, when $\phi = 1$, the effective thermal conductivity will equal that of the solid particles, k_s. Thus, the effective thermal conductivity will have a value between the fluid and solid thermal conductivities. If we have a nanoparticle material that has a higher thermal conductivity than the base fluid, then we can see that the effective thermal conductivity will increase with the volume fraction of particles within the nanofluid.

Due to heat flow being analogous to electrical flow, we can use the thermal resistance of each material to find a total effective thermal conductivity of the system. Given that resistance is the inverse of conductance, we need to minimize its thermal resistance in

order to find the maximum effective thermal conductivity of the nanofluid. Analogous to electrical resistance, the effective thermal resistance of two materials is minimized when the individual resistances are connected in parallel. This allows us to treat the fluid as a system of two materials stacked beside each other, with the particle volume fraction treated as a volume percentage of one material relative to the system. Since the system is characterized by parallel resistances, the corresponding conductances are summed to find the conductivity.

$$k_{eff,max} = \phi k_s + (1 - \phi) k_f \tag{1.3}$$

However, in a case where two materials are stacked in the direction of heat flow, the thermal resistances are configured in series. The thermal resistances are summed accordingly, which maximizes the effective thermal resistance. Given that the conductance of a material is the inverse of its resistance, we can find an expression for the minimum effective thermal conductivity.

$$\frac{1}{k_{eff,min}} = \frac{1}{\phi k_s} + \frac{1}{(1 - \phi) k_f} \tag{1.4}$$

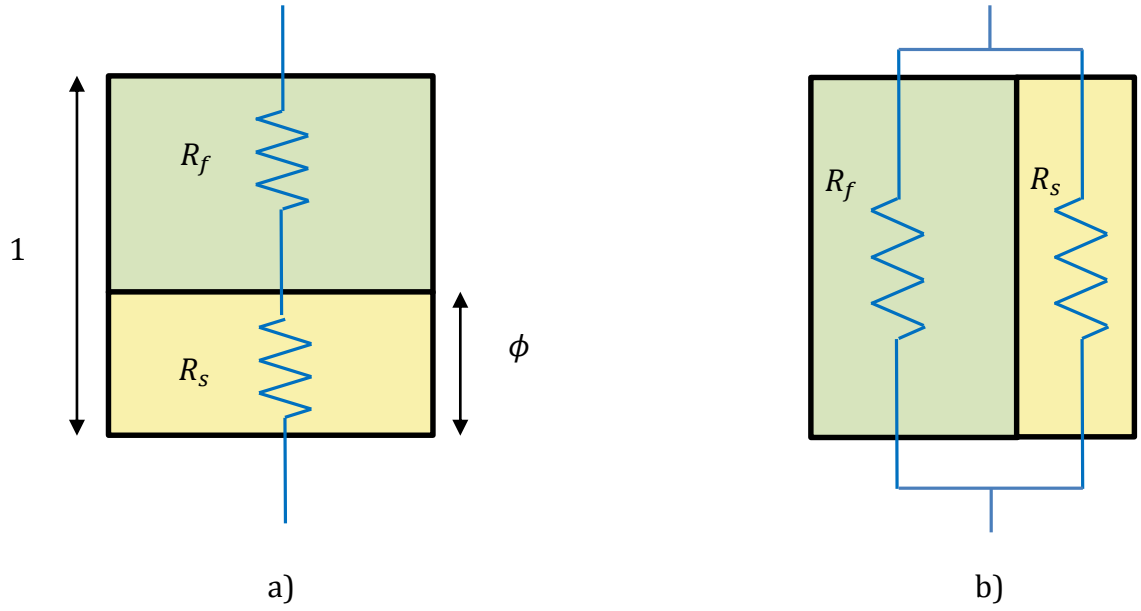

Figure 1.1: Thermal Resistances of two materials in a) series, and b) parallel

1.3 – Magnetism

When charged particles are in motion, they create forces that act on each other due to their motion. These forces are caused by a phenomenon known as magnetism. Similar to forming an electric field due to their charge, these charges form a magnetic field due to their motion. However, unlike the electric field, the magnetic field can do no work, causing the magnetic flux through a closed surface to be zero. Therefore, the

divergence of the magnetic flux density will be zero. This is known as Gauss' Law of Magnetism.

$$\vec{\nabla} \cdot \vec{\mathbf{B}} = 0 \tag{1.5}$$

This implies that a magnetic field cannot exist as a source or a sink point, thus the simplest form it can exist as is a dipole. The convention that is most widely used for identifying magnetic fields is to orient it in a direction that points from a "south" pole to a "north" pole. Due to Gauss' Law of Magnetism, a north pole cannot exist without a south pole.

We can take the magnetic field of a solenoidal electromagnet as an example. A solenoid consists of an electrically conductive wire configured in a helical fashion. The core of the solenoid can contain either air or some magnetic material. Inside of an air-core solenoid the magnetic field is expressed by the following expression.

$$B_z = \frac{\mu_0 NI}{\ell} \tag{1.6}$$

where μ_0 is the permittivity of free space, N is the number of turns in the solenoid, and ℓ is the total length of the solenoid. Given that μ, N, and ℓ are characteristic parameters of the solenoid, we can combine them into a single parameter γ, known as the coil constant.

$$B_z = \gamma I \tag{1.7}$$

We can see that the magnetic field inside of the solenoid is linearly proportional to the current flowing through the wires in the coil. The field outside of the solenoid can be treated as that of a dipole. Combining the fields of these two sections, we are able to find that the magnetic field lines (similar to lines formed at constant values of the stream function) will form closed paths.

1.4 – Magnetic Properties of Nanoparticles

As stated in the previous section, magnetic fields are caused by charged particles in motion, such as that of a current-carrying wire. Although not as evident, this effect can be observed in matter. In the atoms of the material, electrons orbit around their nuclei and also have a certain spin about an axis. These two quantum mechanical phenomena give rise to the notion that charge moves inside matter, thus making it susceptible to manipulation by magnetic forces.

Given that the simplest form a magnetic field can exist is as a single dipole, the magnetic field in matter can be described as a collection of dipoles. The presence of an external magnetic field creates a torque on the dipoles and aligns them to it, defined by their magnetic dipole moment.

$$\vec{\boldsymbol{\tau}} = \vec{\mathbf{m}} \times \vec{\mathbf{B}}_{\mathbf{ext}} \tag{1.8}$$

In matter, we define the magnetic dipole moment per unit volume of the collection of these dipoles as the magnetization of a material. The magnetization field caused by these “bound currents” (electrons bound to each atom) along with an auxiliary field caused by “free currents” (electrons free to travel across the atoms’ outer valence shell) form the total magnetic field outside of the material.[4] This explains how a metal-core solenoid has a stronger outer magnetic field than that of an air-core solenoid.

In nanofluids, each nanoparticle becomes magnetized in the presence of an external magnetic field and creates a small field, in the direction of its average magnetic dipole moment. These small fields interact with each other and the particles attract, forming chains in the direction of the external field.

$$\vec{\mathbf{F}}_{\mathbf{1}} = \vec{\nabla}\left(\vec{\mathbf{m}}_{\mathbf{1}} \cdot \vec{\mathbf{B}}_{\mathbf{2}}\right) \tag{1.9a}$$

$$\vec{\mathbf{F}}_{\mathbf{2}} = \vec{\nabla}\left(\vec{\mathbf{m}}_{2} \cdot \vec{\mathbf{B}}_{\mathbf{1}}\right) \tag{1.9b}$$

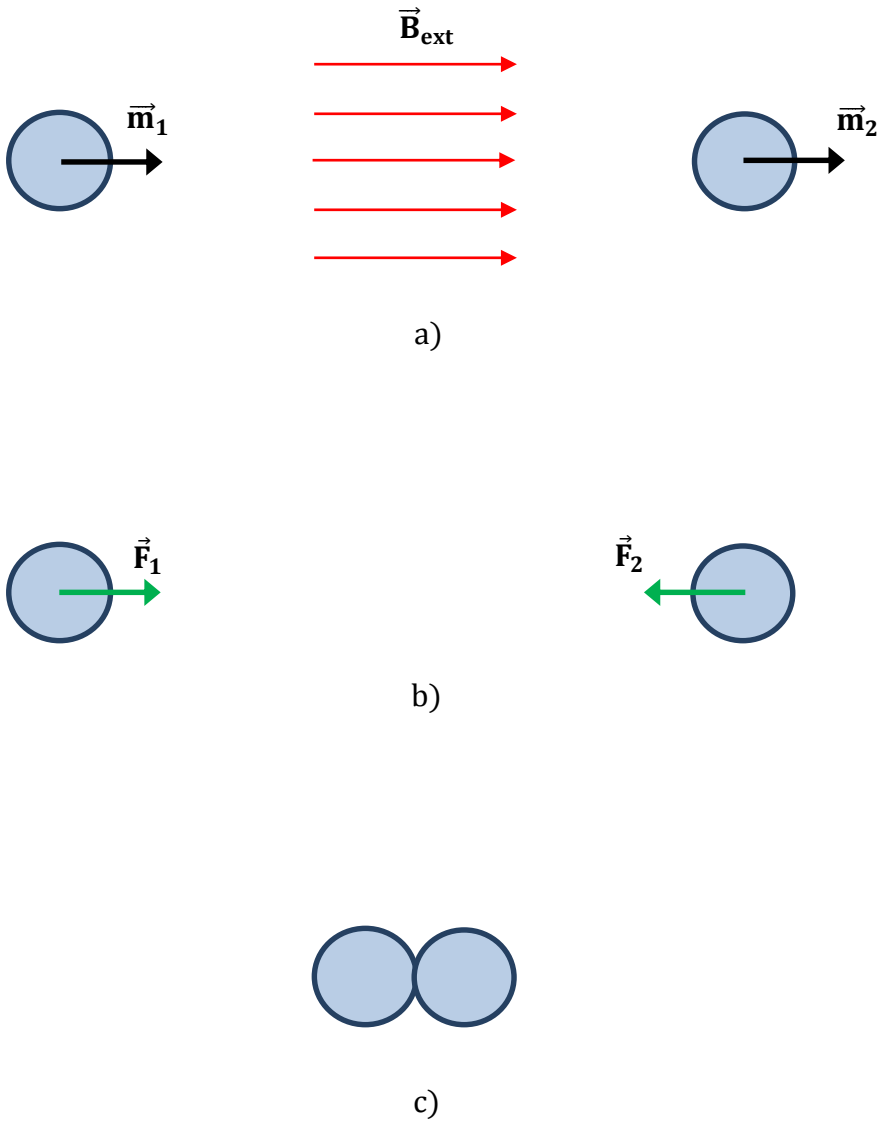

Figure 1.2: External magnetic field induced interaction between two magnetized particles: a) average magnetic dipole moments, b) small magnetic forces acting on each other, c) particles in equilibrium when in contact

The most widely known example of this phenomenon is the alignment of iron filings around a bar magnet. In the figure below, we can see how the iron filings align with the magnetic field created by the bar magnet. The dipole moments of the particles align along the direction of the magnetic field and connect to each other. Also, notice that the greatest concentration of particles is located at the poles of the magnet, where the magnetic field is the strongest.

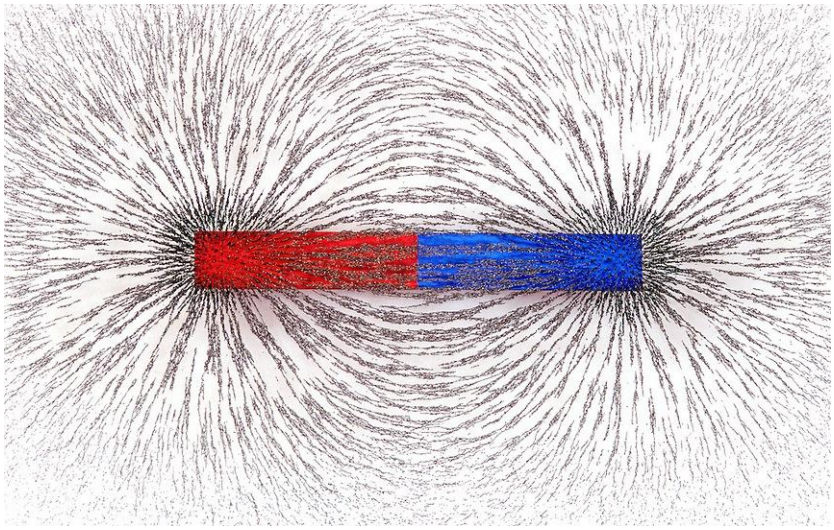

Figure 1.3: Iron filings being used to demonstrate the lines of the magnetic field of a bar magnet

There are three main types of magnetic orientation inside of a material. Paramagnetic materials magnetize parallel to an applied external magnetic field, then demagnetize after the external field is no longer applied. Diamagnetic materials are

similar to paramagnetic materials, but they magnetize antiparallel to the applied field rather than parallel. Ferromagnetic materials magnetize parallel to an external field, but retain magnetization when the field is no longer applied.

1.5 – Purpose of Study

The purpose of this study is to determine if utilizing the magnetic properties of nanofluids will have any effect on thermal conductivity and investigating the cause of why this phenomenon happens. With a thermal conductivity that is able to be fine tuned by external means, we would have more control over heat transfer in any system. With the advancement of technology and its emphasis on the utilization of semiconductor devices packed into the smallest place possible, the traditional bulky heat sinks are struggling to efficiently dissipate the heat that the semiconductor devices generate. Recently, there has been research conducted on liquid cooling of these semiconductor devices. This could possibly replace the metal heat sinks by providing a more efficient heat transfer in a much smaller volume in the future.

Chapter 2

Theory and Experiment Setup

2.1 - Methodology

There have been different methods developed to measure a fluid's thermal conductivity. The most widely used is the transient hot wire method. In this method, a thin resistive wire acts as a heat source vertically inside of some container. The thermal conductivity of the working fluid is calculated using the resistance of the hot wire measured during the time before convection effects can take effect. This is a very effective method for measuring general liquids. However, there arises a problem when attempting to analyze magnetic effects. Ideally, the direction of heat flow should be parallel to the magnetic field. The divergence of heat flow in this case is non-zero due to the heat being sourced from a singular point radially within the container. Gauss' Law of Magnetism states that the divergence of the magnetic flux density is zero, which implies that magnetic fields cannot exist as a singular source or sink point. There have been experiments conducted to where a permanent magnet was placed at a certain distance away from the container, oriented parallel to the direction of heat flow within a certain section of the container.[5] However, since the field of the permanent magnet decreases with distance, it will not provide the uniformity what we desire for the magnetic field.

For this experiment, we require a uniform, unidirectional heat flow to match a uniform, unidirectional magnetic field. To achieve this, we constructed an apparatus consisting of a laterally insulated cylindrical container of height H, which holds the nanofluid. A source of constant heat flux is placed at the top of the container, while the bottom is insulated.

The resulting positive vertical temperature gradient creates a negative vertical density gradient within the fluid. Since the density gradient is in the same direction as the gravitational force, there are no buoyant forces present in the fluid, thus rendering any natural convective effects irrelevant. In turn, the problem is simplified to a one-dimensional conduction problem. Since all the other sides are insulated, there is only one nonhomogeneous boundary condition to consider: the heat transfer due to constant heat flux at the top of the container. This can be described by Fourier's Law at the boundary.

$$q'' = -k \left. \frac{\partial T}{\partial z} \right|_{z=H} \tag{2.1}$$

If we analyze the energy balance throughout the container, we can see that the energy input is coming from the source of constant heat flux. However, since all the other sides of the container are insulated, there will be nowhere for the energy to escape causing a zero energy output. All of the energy from the heat source will be stored inside the liquid. Thus, we cannot expect to find a steady state solution for the temperature distribution.

2.2 – Governing Equation

For any fluid, the equation derived due to conservation of energy is expressed by:

$$\rho c_p \frac{DT}{Dt} = \vec{\nabla} \cdot \left(k\vec{\nabla}T\right) + \frac{\partial p}{\partial t} + \mu\Phi \tag{2.2}$$

On the right hand side, $\mu\Phi$ is the frictional heating term, dependent on the velocity of the fluid. But in this instance, our configuration allows us to neglect any convective effects. Therefore, we can deem the effect of frictional heating negligible. Furthermore, the pressure rate will also be neglected due to the absence of velocity.
Realistically, thermal conductivity is somewhat dependent on temperature, but has very little change within several degrees centigrade, so we can treat it as a constant. This greatly simplifies the problem at hand.

$$\nabla^2 T = \frac{\rho c_p}{k}\frac{\partial T}{\partial t} \tag{2.3}$$

The coordinates used in the equation should follow the geometry of the boundary at hand. Since the container we are using is a cylinder, we will be expressing the energy equation in cylindrical coordinates.

$$\frac{1}{r}\frac{\partial}{\partial r}\left[r\frac{\partial T}{\partial r}\right] + \frac{1}{r^2}\frac{\partial^2 T}{\partial \phi^2} + \frac{\partial^2 T}{\partial z^2} = \frac{\rho c_p}{k}\frac{\partial T}{\partial t} \tag{2.4}$$

To further simplify the equation, we radially insulate the container so the heat will not flow outward. By nature, the cylinder has azimuthal symmetry, so we can neglect the azimuthal term. We will also place a source of constant heat flux in the vertical direction, so the heat flow will only travel in vertical direction. By doing this, we have simplified the

problem from a three-dimensional convection problem to a one-dimensional transient conduction problem.

$$\frac{\partial^2 T}{\partial z^2} = \frac{\rho c_p}{k}\frac{\partial T}{\partial t} \tag{2.5}$$

We set the fluid initially at a uniform temperature T_0. The source of constant heat flux will be placed at the top of the container, and the bottom will be insulated. From this, we can define our initial and boundary conditions.

$$T(z,0) = T_0 \tag{2.6a}$$

$$\left.\frac{\partial T}{\partial z}\right|_{z=0} = 0 \tag{2.6b}$$

$$\left.\frac{\partial T}{\partial z}\right|_{z=H} = \frac{q''}{k} \tag{2.6c}$$

2.3 – Derivation of Working Equation

The main objective for solving this boundary value problem is to manipulate the function in a way that we can easily solve for the temperature distribution by simplifying the boundary conditions.

$$\theta(z,t) = T(z,t) - T_0 \tag{2.7}$$

This represents the temperature change of the fluid relative to its initial temperature. This configuration allows us to manipulate the boundary conditions without disturbing the governing equation.

$$\frac{\partial^2\theta}{\partial z^2} = \frac{\rho c_p}{k}\frac{\partial\theta}{\partial t} \tag{2.8}$$

$$\theta(z,0) = 0 \tag{2.9a}$$

$$\left.\frac{\partial\theta}{\partial z}\right|_{z=0} = 0 \tag{2.9b}$$

$$\left.\frac{\partial\theta}{\partial z}\right|_{z=H} = \frac{q''}{k} \tag{2.9c}$$

The ideal conditions for solving this equation is to manipulate the boundary conditions to where the only non-homogeneity is in the initial condition. To do this, we can separate the function into a summation of smaller functions. We can define two of the terms as functions of each variable, and a third term as a function of both variables.

$$\theta(z,t) = u(z) + v(t) + w(z,t) \tag{2.10}$$

This changes the governing equation and the boundary conditions to where we can separate the ordinary derivatives from the partial derivatives.

$$\frac{d^2u}{dz^2} + \frac{\partial^2 w}{\partial z^2} = \frac{\rho c_p}{k}\left(\frac{dv}{dt} + \frac{\partial w}{\partial t}\right) \tag{2.11}$$

$$v(0) + w(z,0) = 0 \tag{2.12a}$$

$$u'(0) + \left.\frac{\partial w}{\partial z}\right|_{z=0} = 0 \tag{2.12b}$$

$$u'(H) + \left.\frac{\partial \theta}{\partial z}\right|_{z=H} = \frac{q"}{k} \tag{2.12c}$$

Solving for $u(z)$ and $v(t)$, we obtain the ideal conditions to solve for $w(z,t)$. After solving the boundary value problem and all the constants of integration, we end up with expressions for each function.[6]

$$u(z) = \frac{q"}{2kH}\left(z^2 - \frac{H^2}{3}\right) \tag{2.13a}$$

$$v(t) = \frac{q"}{\rho c_p H}t \tag{2.13b}$$

$$w(z,t) = \frac{2q"H}{k}\sum_{n=1}^{\infty}\frac{(-1)^{n+1}}{(n\pi)^2}\cos\left(\frac{n\pi z}{H}\right)\exp\left(-\frac{k(n\pi)^2}{\rho c_p H^2}t\right) \tag{2.13c}$$

From Equation 2.10, we can obtain a complete expression for the temperature change in the fluid.

$$\theta(z,t) = \frac{q"}{\rho c_p H}t + \frac{q"}{2kH}\left(z^2 - \frac{H^2}{3}\right) + \frac{2q"H}{k}\sum_{n=1}^{\infty}\frac{(-1)^{n+1}}{(n\pi)^2}\cos\left(\frac{n\pi z}{H}\right)\exp\left(-\frac{k(n\pi)^2}{\rho c_p H^2}t\right) \tag{2.14}$$

Using this expression, we can find the temperature measured at each boundary.

$$\theta(0,t) = \frac{q"}{\rho c_p H}t - \frac{q"H}{6k} - \frac{2q"H}{k}\sum_{n=1}^{\infty}\frac{(-1)^{n}}{(n\pi)^2}\exp\left(-\frac{k(n\pi)^2}{\rho c_p H^2}t\right) \tag{2.15a}$$

$$\theta(H,t) = \frac{q"}{\rho c_p H}t + \frac{q"H}{3k} - \frac{2q"H}{k}\sum_{n=1}^{\infty}\frac{1}{(n\pi)^2}\exp\left(-\frac{k(n\pi)^2}{\rho c_p H^2}t\right) \tag{2.15b}$$

After a long period of time, the temperature change will linearize due to the diminishing effect of the summation term. Therefore, since the other terms remain constant, the difference in temperature between the top and bottom boundaries will converge to a particular value. We can define a function to describe the temperature difference.

$$\Delta(t) = \theta(H,t) - \theta(0,t) \tag{2.16}$$

Notice that the first term in Equations 2.15a and 2.15b are equal, so the linear terms will simplify into a constant.

$$\Delta(t) = \frac{q"H}{k}\left[\frac{1}{2} + 2\sum_{n=1}^{\infty}\frac{1-(-1)^n}{(n\pi)^2}\exp\left(-\frac{k(n\pi)^2}{\rho c_p H^2}t\right)\right] \tag{2.17}$$

When time becomes large, the summation term vanishes, causing the temperature difference to converge to a constant, steady state-like value.

$$\Delta_{ss} = \frac{1}{2}\frac{q"H}{k} \tag{2.18}$$

Finally, we can extract the thermal conductivity of the fluid from the expression of the steady state temperature difference.

$$k = \frac{1}{2}\frac{q"H}{\Delta_{ss}} \tag{2.19}$$

We created a Finite Difference Model of the problem in order to easily visualize the temperature distribution inside the container over space and time. The parameters we used for the model were the fluid properties of pure water (density: $1000\ \mathrm{kg/m^3}$, specific heat: $4180\ \mathrm{J/kg\,K}$, thermal conductivity: $0.6\ \mathrm{W/m\,K}$)[7], constant heat flux value at $200\ \mathrm{W/m^2}$, and the cylinder height at $0.05\ \mathrm{m}$. A 5 millimeter spacing and a 60 second time step was used in the finite-difference equations.

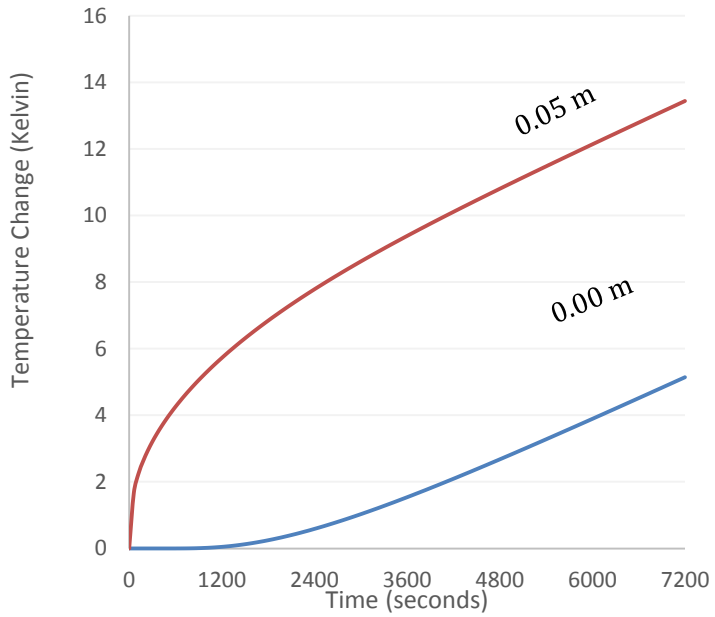

Figure 2.1: Finite Difference Model of the Temperature Change at the top and bottom boundaries vs. Time

A time duration of 120 minutes was used to show the linearity of the temperature change at a large time. The coefficient of the time-dependent term (the second term in Equation 2.10) serves as the slope of the linear region, which is dependent on the density and the specific heat of the fluid. Since it is the same for both the top and bottom temperature distributions, it is easy to see that the temperature difference between the top and bottom boundaries converges to a single value at a large time.

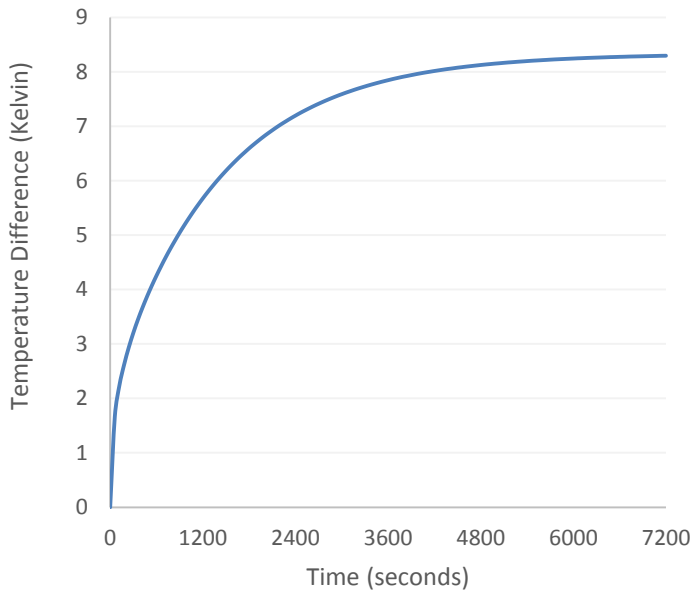

Figure 2.2: Finite Difference Model of the Temperature Difference between the top and bottom boundaries vs. Time

As for the spatial distribution, we can see how the heat flows throughout the container but never settles to a steady state distribution. When the system linearizes, the shape of the

spatial distribution matures into some sort of pseudo-steady state distribution. At this point, all the values of temperature increase with time at the same rate.

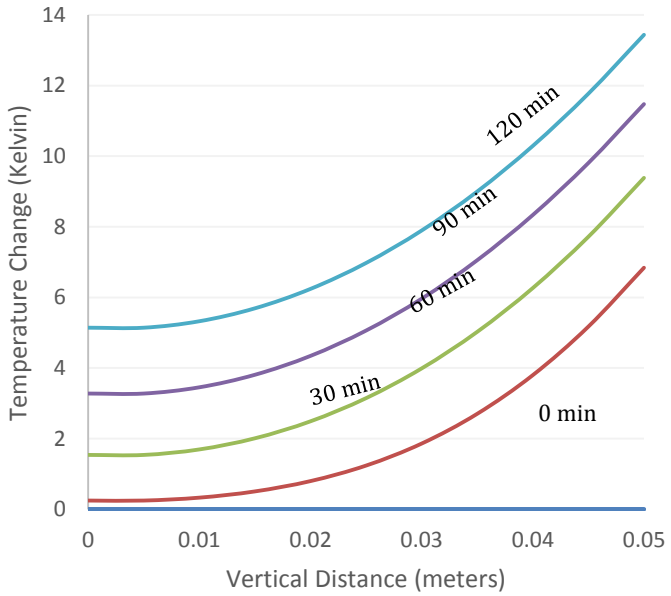

Figure 2.3: Finite Difference Model of the Temperature Difference between the top and bottom boundaries vs. Vertical Distance

The heat flux of the system, however, has a different behavior. We can apply Fourier's Law to the temperature distribution stated in Equation 2.14 to obtain the heat flux distribution.

$$q''(z,t) = q''\frac{z}{H} + 2q''\sum_{n=1}^{\infty}\frac{(-1)^n}{n\pi}\sin\left(\frac{n\pi z}{H}\right)\exp\left(-\frac{k(n\pi)^2}{\rho c_p H^2}t\right) \tag{2.20}$$

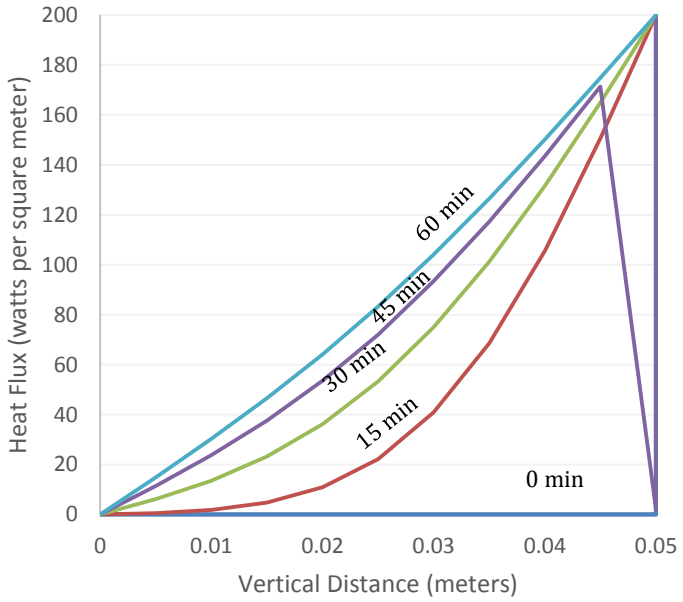

Figure 2.4: Finite Difference Model of the Heat Flux Distribution between the top and bottom boundaries vs. Vertical Distance

As we can see from Figure 2.4, The heat flux distribution becomes steady state at a large time. When the heat flux becomes steady state, the temperature distribution linearizes at every point with time. Thus, the temperature difference converges and we can extract the thermal conductivity from the expression in Equation 2.19.

2.4 – Description of Apparatus

In order to execute this experimentally, we configured a container with a circular electric wire heater placed on the underside of the cap. Since the resistivity of a material increases with temperature, the heater was made from nichrome wire to ensure a constant heat flux, due to its significantly low temperature coefficient of resistivity. In order to create a uniform magnetic field, we constructed a copper-wire solenoidal electromagnet that surrounded the nanofluid container. The electromagnet, powered by a Hewlett Packard 6038A DC Power Supply, was oriented in such a way that its magnetic field lines run parallel to the direction of heat flow.

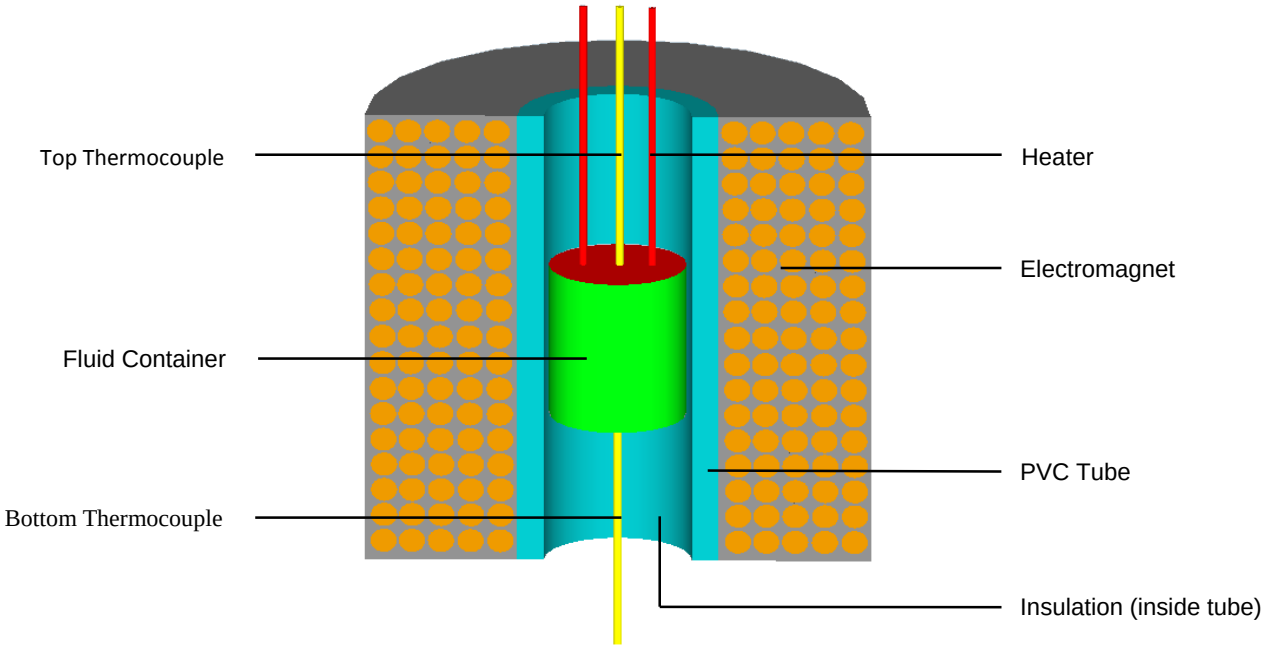

Figure 2.5: Cross-Sectional View of the Main Apparatus

Two thermocouples were configured on the cap where the heater was placed, and bottom of the container to measure the temperature at those two points. The thermocouples were connected to a Keithley 2700 Digital Multimeter (DMM), which enabled us to read the temperature in degrees centigrade. The DMM transferred data from the thermocouples to a LabVIEW program. Using the program, the temperature difference between the two thermocouples was calculated and the data was written into a Microsoft Excel spreadsheet via LabVIEW and plotted over time.

A benefit of using this method of thermal conductivity measurement is that we are able to neglect any convective effects due to the nature of the setup. This allows us to consider only the conduction of the system; the temperature range is low (around room temperature), therefore we can also neglect any radiative effects. Also, we are able to control a uniform magnetic field that is parallel to a uniform heat flow. When the system is one-dimensional, uniform, and unidirectional, the problem becomes extremely simple. However, this method requires a rather large duration of measurement, whereas each measurement in the transient hot wire method occurs over only a few seconds. Alas, the benefits of this method are well worth the time required for each measurement.

Chapter 3

Experiment and Discussion

3.1 – Procedure

We prepared four different nanofluids: Aluminum (III) Oxide (Al2O3, diamagnetic, 80 nm diameter), Copper (II) Oxide (CuO, paramagnetic, 40 nm diameter), Iron (II, III) Oxide (Fe3O4, ferrimagnetic, 20-30 nm diameter), and Silicon (IV) Oxide (SiO2, diamagnetic, 20-30 nm diameter). Each nanofluid was stabilized with a sodium dodecyl sulfate (SDS) surfactant, and was prepared at a volume fraction of 0.125 by adding 5 milliliters of nanoparticles to 35 milliliters of the water-surfactant solution. The electromagnet was constructed from 294 meters of 12 Gauge copper wire and a 1 ½ inch PVC pipe. 709 turns of the wire were wrapped around the PVC pipe to form the solenoid at a height of 14 centimeters, which characterized the electromagnet with a coil constant of $63.8\ \mathrm{G/A}$. The electromagnet was oriented in such a way that the magnetic field was pointed upward, antiparallel to the direction of heat flow and gravitational acceleration. The heater was constructed from 1.2 meters of 26 Gauge nichrome wire in a spiral with an outside diameter of 3.2 centimeters to fit inside the container. The wire heater was powered by a Duracell MN908 6-volt battery with a toggle switch and five $150\ \Omega$ resistors in parallel for a total of 30 ohms in order to limit the current through the heater.

We tested each nanofluid by applying heat from the heater and measuring the temperature difference after it converged to a single value. In order to measure the temperature difference accurately, we conducted each measurement over the course of

one hour. After the hour of measurement, the heater was turned off and the temperature difference was recorded. Before each measurement, the nanofluid was brought back to equilibrium conditions by stirring it back to room temperature. This ensured a consistent measurement throughout the course of the experiment. We used this method to calibrate the apparatus by using deionized water at room temperature, which has a known thermal conductivity of $0.6\,\mathrm{W/m\,K}$. Given a known thermal conductivity, we were able to calculate the heat flux that the heater provided as $260\ \mathrm{W/m^2}$. We conducted six measurements with each nanofluid. The first measurement was performed with no effect from the magnetic field, then the electromagnet was turned on and increased by 2-amp increments for a magnetic field increment of 127.6 Gauss. The electromagnet was powered to a maximum of 10 amps for the sixth measurement in each nanofluid. With six measurements in each of the four nanofluids, we conducted a total of 24 measurements.

3.2 – Results & Discussion

The experiment apparatus performance was nearly identical to the theoretical scenario described in Chapter 2. The figure below shows the transient temperature as a function of time for the iron oxide nanofluid under the influence of a magnetic field that has a strength of 255.2 Gauss.

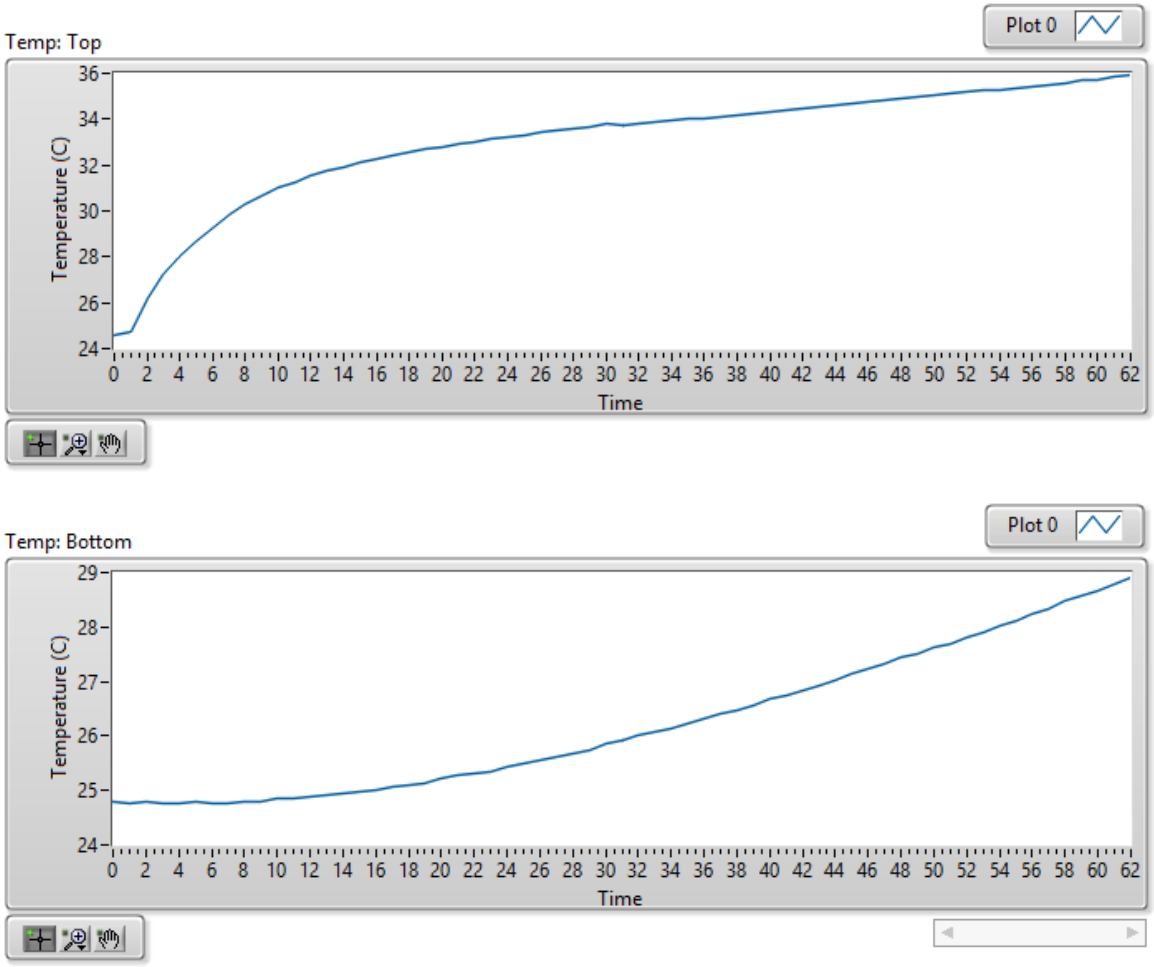

Figure 3.1: Transient temperature of 12.5% volume fraction Fe_3O_4 with a 255.2 Gauss applied magnetic field: measured at the top and bottom thermocouples over time. Data retrieved from LabVIEW.

In this case, the heater was turned on at 1 minute into the measurement. The shape of the temperature vs. time graph is consistent with the finite difference method description of the theoretical model in Figure 2.1, so this shows that this measurement method is valid. The temperature differences for each of the 24 measurements were recorded and analyzed.

Table 3.1: Measured Temperature Difference for each nanofluid with various magnetic field strengths

Magnetic Field	Temperature Difference (K)			
(Gauss)	Al2O3	CuO	Fe3O4	SiO2
0	7.71971	7.64615	9.29794	9.52108
127.6	5.93585	5.60441	7.97141	8.48898
255.2	1.98777	3.34173	6.99433	6.80422
382.8	1.66577	1.7651	5.67032	5.95806
510.4	1.42631	1.31974	5.00351	5.72037
638	1.32561	1.04493	4.39606	5.48342

We can see that the temperature difference decreases as the strength of the magnetic field increases. As described in the relation in Equation 2.19, the thermal conductivity is inversely proportional to the temperature difference. Therefore, we can see that the thermal conductivity does in fact increase as an external magnetic field increases.

Table 3.2: Thermal Conductivity calculated from the measured Temperature Difference for each nanofluid with various magnetic field strengths

Magnetic Field (Gauss)	Thermal Conductivity (W/(m K))			
	Al2O3	CuO	Fe3O4	SiO2
0	0.84200	0.85010	0.69907	0.68269
127.6	1.09504	1.15980	0.81541	0.76569
255.2	3.26999	1.94510	0.92932	0.95528
382.8	3.90209	3.68251	1.14631	1.09095
510.4	4.55720	4.92521	1.29908	1.13629
638	4.90340	6.22051	1.47859	1.18539

The value of thermal conductivity with no applied magnetic field our experimental value of k_0, the thermal conductivity of the nanofluid at its suspended equilibrium. From this, we

can manipulate the relation in Equation 1.2 to find the experimental value of the thermal conductivity of the nanoparticles.

Table 3.3: Calculated thermal conductivity of solid nanoparticles, and the Maxwellian thermal conductivity of each nanofluid

	$k_0 \left(\mathrm{W}/_{\mathrm{m\ K}}\right)$	$k_s \left(\mathrm{W}/_{\mathrm{m\ K}}\right)$	$k_{s,known} \left(\mathrm{W}/_{\mathrm{m\ K}}\right)$[8 9 10]
Al2O3	0.84200	33.477	30
CuO	0.85010	73.663	78
Fe3O4	0.69907	1.889	Unknown
SiO2	0.68269	1.575	1.4

Notice that the copper oxide and aluminum oxide nanoparticles have a much greater thermal conductivity than the iron oxide and the silicon dioxide nanoparticles. This can explain the greater increase of thermal conductivity in the copper oxide and the aluminum oxide as opposed to the smaller increase in thermal conductivity in the iron oxide and the silicon dioxide.

We can describe the enhancement as a ratio of the measured thermal conductivity over the thermal conductivity of the base fluid. This shows that the thermal conductivity is

enhanced by simply adding a concentration of nanoparticles to the base fluid, given that the thermal conductivity of the particles is greater than the thermal conductivity of the base fluid.

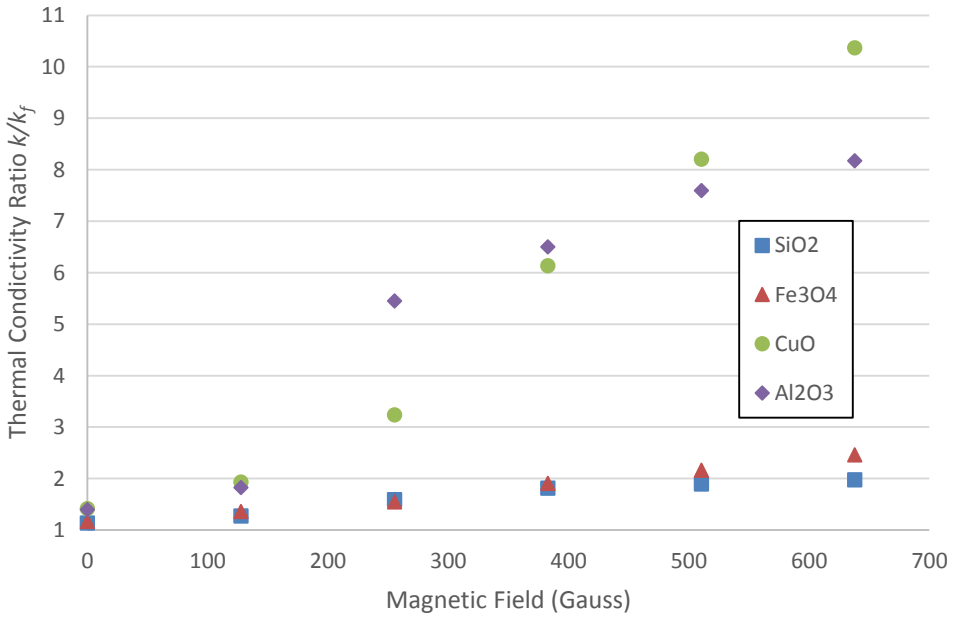

Figure 3.2: Thermal conductivity ratio of each nanofluid vs. magnetic field strength

We can more easily see the enhancement of thermal conductivity by defining a relative thermal conductivity enhancement κ. This dimensionless quantity can be described as the ratio of the enhanced thermal conductivity over the maximum thermal conductivity

relative to the non-enhanced thermal conductivity. The relative enhancement will be at 1 when at maximum, and at 0 when non-enhanced.

$$\kappa = \frac{k - k_0}{k_{max} - k_0} \tag{3.1}$$

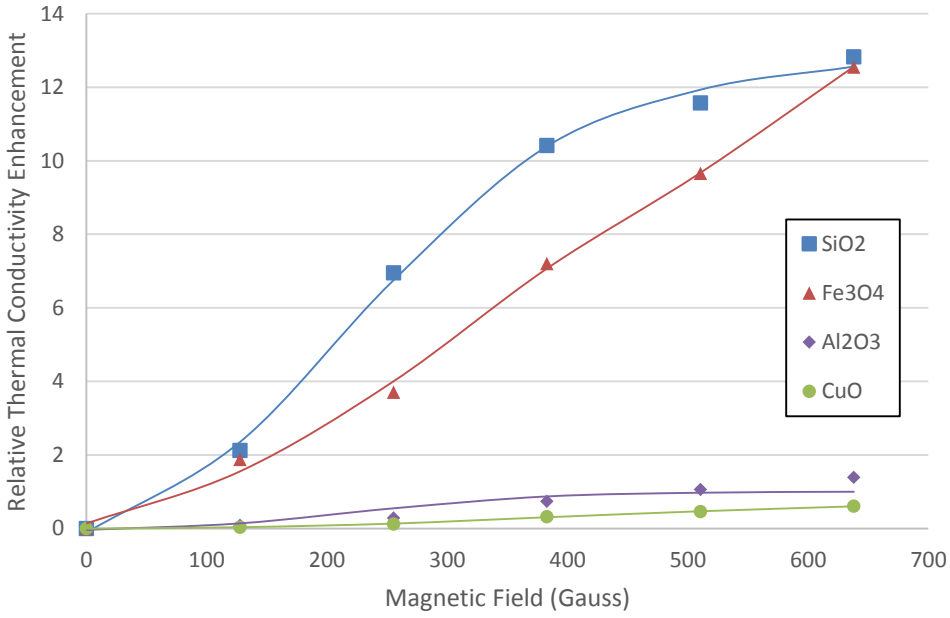

Figure 3.3: Relative thermal conductivity enhancement of each nanofluid vs. magnetic field strength

The shape of the data somewhat resembles a hyperbolic tangent function. We can analyze the data by comparing it to a parameterized function.

$$\kappa(B) = a + b\tanh(cB - d) \tag{3.2}$$

where a, b, c, and d are parameter constants specific to each nanofluid. When at maximum, $\kappa = 1$, and when at minimum, $\kappa = \kappa_{min}$. When the nanofluid is not being subject to a magnetic field, $\kappa = 0$. The relative enhancement seems to experience a point of inflection at a certain strength of magnetic field, which the thermal conductivity will be at its average value between the maximum and minimum values. Applying these conditions to Equation 3.2, we find expressions for the parameter constants as a function of the critical relative enhancement values.

$$a = \frac{1 + \kappa_{min}}{2} \tag{3.3a}$$

$$b = \frac{1 - \kappa_{min}}{2} \tag{3.3b}$$

$$d = \operatorname{arctanh}\frac{1 - \kappa_{min}}{1 + \kappa_{min}} \tag{3.3c}$$

Inputting the expressions into the parameters in Equation 3.2, we obtain a relation for the relative thermal conductivity enhancement as a function of magnetic field and the nanofluid characteristics. By the Least Squares Method of curve fitting, we can determine the value for each coefficient in each of the nanofluids.

$$\kappa(B) = \frac{1 + \kappa_{min}}{2} + \frac{1 - \kappa_{min}}{2}\tanh\left(cB - \operatorname{arctanh}\frac{1 - \kappa_{min}}{1 + \kappa_{min}}\right) \tag{3.4}$$

Table 3.4: Coefficients and constants in the suggested hyperbolic tangent function for each nanofluid

	a	b	$c\ (\mathrm{G}^{-1})$	d
Al2O3	0.455239458	0.544513689	0.006539845	1.496263935
CuO	0.290306234	0.311534479	0.004718452	1.758431519
Fe3O4	5.777211228	6.796580476	0.003604584	1.187479438
SiO2	5.652393785	6.911375166	0.005329344	1.199936996

Given that the system will maximize at $\kappa_{max} = a + b$, we can see that the experimental relative enhancement values differ from our expectation. Both the silicon dioxide and iron oxide nanofluids were over twelve times the relative maximum, whereas the copper oxide actually was about 60 percent of the relative maximum. Notice that both silicon dioxide and iron oxide have thermal conductivities closer to that of the base fluid, thus the difference in thermal conductivity of each constituent in the nanofluid is rather small. Whereas aluminum oxide and copper oxide have much larger thermal conductivities than their corresponding base fluid. The thermal conductivity difference between the particles and the base fluid tends to have an inverse proportionality to the relative enhancement scaling that we see in the experimental case. If we divide the relative enhancement by the experimental maximum, $a + b$, we can further analyze the behavior of the thermal conductivity.

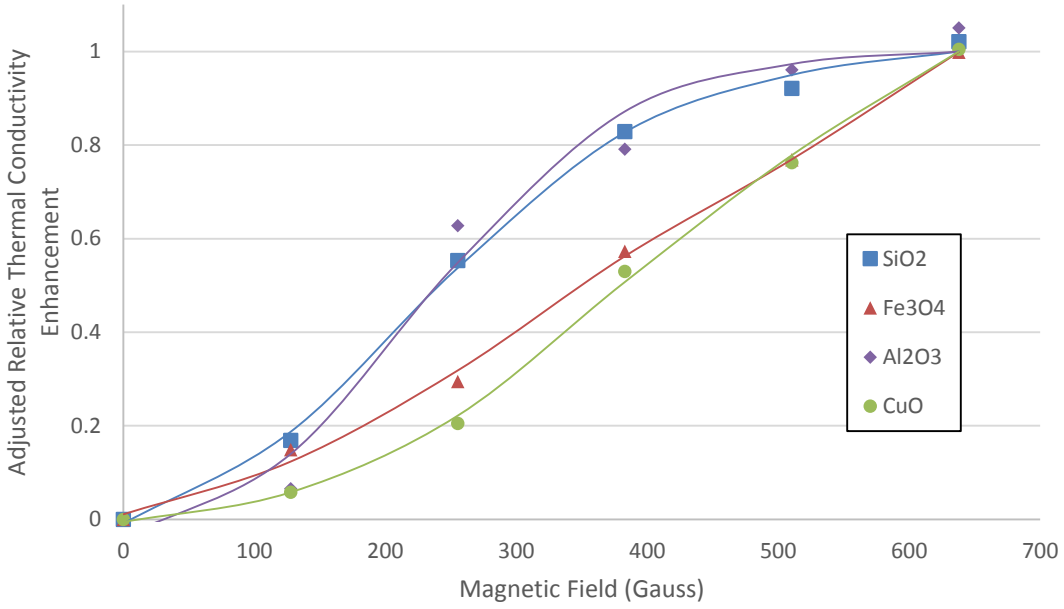

Figure 3.3: Adjusted relative thermal conductivity enhancement of each nanofluid vs. magnetic field strength

From here, we can see where each point of inflection occurs in the relative enhancement, and there exists a critical point in the magnetic field to where this inflection occurs, defined by B_c. By nature of the hyperbolic tangent function, the inflection occurs at the point where the argument of the hyperbolic tangent function is zero.

$$B_c = \frac{1}{c}\operatorname{arctanh}\frac{1-\kappa_{min}}{1+\kappa_{min}} \tag{3.5}$$

Table 3.5: Critical Magnetic Field of each nanofluid compared with the magnetic susceptibility of the particles and the slope coefficient of thermal conductivity

	B_c (Gauss)	χ_m [11 12]	c (G^{-1})
Al2O3	184.698	-3.700 x 10^{-5}	0.006539845
CuO	354.423	+2.596 x 10^{-4}	0.004718452
Fe3O4	348.505	1.2 - 19	0.003604584
SiO2	215.835	-2.96 x 10^{-5}	0.005329344

The above table shows the critical magnetic field alongside the magnetic susceptibility and the slope coefficient inside the argument of the hyperbolic tangent function for comparison. The particles with the highest magnetic susceptibility, copper oxide and iron oxide, have the least effect on the slope coefficient, but have the highest critical magnetic field. It should be noted, however, that these materials are paramagnetic and ferrimagnetic, respectively. They align parallel to the magnetic field, which is oriented against gravitational acceleration. Whereas the aluminum oxide and the silicon dioxide are diamagnetic and align antiparallel to the magnetic field and along with gravitational acceleration. When the magnetic field is aligned against gravitational acceleration, the paramagnetic and ferrimagnetic particles seem to require a stronger magnetic field to overcome gravitational forces than the diamagnetic particles. Therefore, the critical magnetic field may represent the field at which magnetic forces and gravitational forces are equal.

We can see from the previous table that the slope coefficient decreases as the magnetic susceptibility increases, causing the correlation to become more linear in nature. We can see some sort of inverse relationship between the slope coefficient and the magnetic susceptibility. With the slope coefficient being a function of magnetic susceptibility and the horizontal shift component of the hyperbolic tangent function argument being a function of the maximum and minimum thermal conductivities, the critical magnetic field can be found as dependent on all three of these quantities.

Chapter 4

Conclusions

4.1 – Conclusions

We have completed our objective and confirmed that a magnetic field parallel to heat flow does indeed enhance the thermal conductivity of magnetic nanofluids. Although the results did not fully follow the thermal resistance model predicted in Chapter 1, we were able to obtain a somewhat empirical expression of the thermal conductivity as a function of the external magnetic field.

$$k(B) = \Lambda(k_s, k_f)\left\{\frac{k_{max} + k_{min}}{2} + \frac{k_{max} - \kappa_{min}}{2}\tanh\left(c(\chi_m)B - \operatorname{arctanh}\frac{k_{max} - k_{min}}{k_{max} + k_{min}}\right)\right\} \tag{4.1}$$

Also, by completely eradicating convective effects in the fluid, we have confirmed the validity of a rather unique method of measuring thermal conductivity of a fluid.
With the most common method being the transient hot wire method, this would provide an alternative when the experiment requires conditions beyond the restrictions of the transient hot wire apparatus.

Due to the large density ratio between the particles and the base fluid, particle settling posed a potential problem, especially with the large duration of measurement. Without the stabilization of the particles in the fluid by a surfactant, the particles would

settle to the bottom of the container and completely separate from the fluid. This effect would have shown up in the thermal conductivity measurement due to the thermal resistances configuring in series. This would be the case of minimum thermal conductivity described in Chapter 1, where we would have seen a rather large measurement in temperature difference. We did not see this effect show up in the experiment, as we only saw enhancement when the magnetic field was applied and the equilibrium measurement was nearly identical to the Maxwell equation of effective thermal conductivity.

4.2 – Future Work

In order to utilize this theory in various applications, we will need to form a more complete understanding of the behavior of the thermal conductivity of various nanofluids under the influence of an external magnetic field. There are a large number of parameters that can be adjusted in this experiment alone. For instance, we can vary the base fluid rather than vary the particles. This will provide more information on the scaling of the relative enhancement due to the differences between the thermal conductivity of the particles and the base fluid. In the conducted experiment, we found that the thermal conductivity maximizes when the magnetic field is parallel to the direction of heat flow due to the parallel connection of the thermal resistances. If the thermal conductivity minimizes when the thermal resistances align in series, then we can theorize that this would be the case if the magnetic field is perpendicular to the direction of heat flow. If this is true, then we can

vary the angle between the direction of magnetic field and the direction of heat flow, which can possibly be described by the following relation.

$$k_{eff} = k_{min} + (k_{max} - k_{min})|\cos\psi| \tag{4.2}$$

where ψ is the angle between the magnetic field and heat flow directions, at a maximum of 90 degrees.

The conditions of this experiment were set as uniform distributions, unidirectional fields, and constant values in order to make the experiment as simple as possible. To further delve into the study, we would need to look into using a variable, non-uniform magnetic field to see how heat is directed through the fluid in different directions, as well as different geometries for the heat source input. Powering an electromagnet with AC current would produce interesting results due to the rapidly changing magnetic field; the fluid might heat itself by means of magnetic induction inside the particles.

We would be able to extend the study into analyzing heat transfer effects in convection. With the conductivity studies, we gave traditionally solid properties to a fluid that it would not normally have. But in convection, we would give fluid properties to solid particles that they would not normally have due to a solid's inability to flow. By exposing the effect of the magnetic properties of the fluids on thermal conductivity and along with rheological studies on viscosity enhancement by magnetic field, we can have a fluid enhanced with solid properties flow so that the solid properties would then be enhanced when the fluid is in motion. For example, a higher thermally conductive fluid would cause a relatively higher convective heat transfer coefficient in a system. Having the nanofluid

flow through a series of microchannels would even greater enhance the convective heat transfer in the system.

We can use this technology in a large number of heat transfer applications remove heat from semiconductor devices at an extremely high efficiency. The implementation of this technology would replace the traditional bulky metal heat sinks, and change the way we use heat transfer in the future.

References

1. The Science of Nanofluids, Cool-X Nanofluid Technology, (www.cool-x.com)
2. Maiga, S. E. B., Palm, S. J., Nguyen, C. T., Roy, G., Galanis, N. (2005). "Heat transfer enhancement by using nanofluids in forced convection flows". International Journal of Heat and Fluid Flow, 26: 530–546
3. Bergman, T. L, Lavine, A. S., Incropera, F. P., Dewitt, D. P. (2011). Fundamentals of Heat and Mass Transfer. 120, 121
4. Griffiths, D., (1999). Introduction to Electrodynamics. 262
5. Nikapitiya, N. Y. J. B., Moon, H. (2012). “Thermal Conductivity Enhancement of Room Temperature Ionic Liquids (RTILS) with Various Magnetic Particles“.
6. Drake, S. J., Wetz, D. A., Ostanek, J. K., Miller, S. P., Heinzel, J. M., Jain, A., “Measurement of anisotropic thermophysical properties of cylindrical Li-ion cells”, J. Power Sources, 252: 298-304.
7. Bergman, T. L, Lavine, A. S., Incropera, F. P., Dewitt, D. P. (2011). Fundamentals of Heat and Mass Transfer. 1004
8. Material Properties Data: Alumina (Aluminum Oxide), www.makeitfrom.com
9. Anandan, A., Rajan, K. S. (2012). “Synthesis and Stability of Cupric Oxide-based Nanofluid: A Novel Coolant for Efficient Cooling”. Asian Journal of Scientific Research, 5: 218-227
10. Properties: Silica – Silicon Dioxide (SiO2), AZO Materials (www.azom.com)
11. Magnetic Properties and Susceptibilities Chart, READE Advanced Materials (www.reade.com)
12. Classes of Magnetic Materials (irm.umn.edu)

Biographical Information

Christopher Allen was raised in San Angelo, Texas, where he obtained his Bachelor of Science in Physics from Angelo State University. He then moved to Arlington, Texas to pursue graduate studies. He earned a Master of Science in Mechanical Engineering from the University of Texas at Arlington, with an emphasis in the thermal sciences in the areas of heat transfer and thermodynamics. He has hopes of pursuing a career in the defense industry designing military weapons, vehicles, aircraft, and other defense systems that are necessary for the protection of our Nation.